Journal of Solid Mechanics Vol. 12, No. 4 (2020) pp. 902-911
DOI: 10.22034/jsm.2020.1899251.1587

Fatigue Crack Growth in Plastically Compressible Solids: Role of Negative Stress Ratio, Plastic Compressibility and Strain Softening

Y. Mittal, D. Khan*, S. Pandey, G. Chand Gupta

Department of Mechanical Engineering, Indian Institute of Thechnology Varansi, Varansi, India

Received 30 July 2020; accepted 3 October 2020

ABSTRACT

The effect of cyclic loading on fatigue crack growth in plastically compressible solids is investigated at negative stress ratio under plane strain and small scale yielding conditions. The material is characterized by a finite strain elastic viscoplastic constitutive model with hardening and hardening-softening-hardening hardness functions. Displacements corresponding to the isotropic linear elastic mode I crack field are prescribed on a remote boundary. The plastic crack growth, crack tip opening displacement (CTOD) and near crack tip stress fields are presented using finite element method. Material hardening/ softening has a major relevance on crack growth, CTOD and the evolution of stress distribution. It is revealed here that the negative stress ratio can significantly influence the loading conditions at the crack tip and thereby increase the crack growth for tension–compression loading for hardening material whereas the fatigue crack growth of plastically compressible hardening-softening-hardening material is only slightly affected by the negative stress ratio albeit it is accepted in literature that compressive loads contribute to fatigue crack growth significantly. In the present studies, the CTOD variation with applied load and the near stress distribution are also very unusual in nature.

Keywords: Compressible solids; Fatigue crack growth; Finite element method; Material softening; Negative stress ratio.

1 INTRODUCTION

CRACK driving force in fatigue crack growth is to a great extent smaller than the driving force required for the same crack to grow under monotonic loading. There have been incessant endeavors to achieve the salient results of fatigue crack growth for small as well as large deformation formulations. Earlier people used to ignore the contribution of the compressive load part of the fatigue load cycle with the assumption that fatigue crack tip remains closed during compression loading and there is no stress concentration around the crack. Also, in literature difference between positive and negative stress ratios in relation to fracture is not presented separately most of the

*Corresponding author. Tel.:+91 983 8445007; Fax.: +91 542 2368157.
E-mail address: dkhan.mec@itbhu.ac.in (D. Khan).

times. However, in the last decades, a few works reported that during tension-compression loading, compression loading effect on fatigue crack growth could not be ignored and it played an important role in the growth phenomena, [1-5]. However, most of the studies are experimental in nature and only a few theoretical/ simulation research works are available towards this direction. Effort has also been made to study the fatigue crack growth for tension-shear specimens based on the calculation of stress intensity factors and *J*-integral using three-dimensional finite element method [6]. As well for positive stress ratio, the role of microstructural parameters on fatigue crack growth has been investigated in [7]. To the best of the authors' knowledge, so far such fatigue crack growth studies at negative stress ratio have been performed with materials like steels, aluminum alloys, titanium alloys etc and similar investigations for relatively new materials like metallic foam, toughened structural polymers, transformation toughened ceramics etc. are not available in the open literature. These new materials possess a number of excellent mechanical properties, like high viscoelastic energy absorption, very good compliant thermal interfaces, biomimetic dry adhesives etc. Experiments have revealed that the constitutive equations of these materials accounts for pressure-dependent yielding. Numerous studies have been carried out over the past several years to understand the near tip deformation as well as stress-strain fields of such plastically compressible/ incompressible materials under monotonic and cyclic loading, [8-15]. The material softening is very common in the constitutive behavior of metallic foams, vertically aligned carbon nanotubes (VACNTs) and polymeric materials, [13, 16]. Very recently, a mode I crack subjected to cyclic loading (with constant amplitude and zero as well as positive stress ratios) has been investigated with some basic results for plastically compressible hardening and hardening-softening-hardening solids using the crack tip blunting model in [17]. But for plastically compressible materials and when there is material softening in the hardness function, up to what extent the compressive load contributes the fatigue crack growth has not been looked into by the previous researchers till now. Also, how the negative stress ratio affects the crack growth in hardening material differently as compared to that of materials contains strain softening has not been addressed by the research community so far.

Therefore, considering the prospective uses of the comparatively new materials as mentioned above and their incomplete exploration till now, an attempt has been made here to explore the behavior of a mode I crack in bilinear hardening and hardening-softening-hardening materials following isotropic, plastically compressible rate dependent elastic viscoplastic constitutive relation under cyclic loading at negative stress ratio. Both constant amplitude as well as variable amplitude loading with a single overload have been considered for simulation. Here, solid with hardening-softening-hardening responses has been considered as such behavior can occur for metallic foams and VACNTs. Also, under identical conditions, for comparison purpose, the behavior of a hardening material is considered as it can occur for metals. The present computations are limited to plane strain, small scale yielding and plastic normality flow rule.

2 THEORETICAL FRAMEWORK

The constitutive relation used here is based on writing the rate of deformation tensor, $\mathbf{d}$ is the sum of isotropic elastic part $\mathbf{d}^e = \mathbf{L}^{-1}:\hat{\boldsymbol{\tau}}$ characterized by Young's modulus E and Poisson's ratio ν and a viscoplastic plastic part $\mathbf{d}^p$. Elastic strains are assumed to be very small. The plastic part of the response is given in [17] as:

$$\mathbf{d}^p = \frac{3}{2}\frac{\dot{\varepsilon}_p}{\sigma_e}\mathbf{p} \tag{1}$$

where,

$$\mathbf{p} = \tau - \alpha tr(\tau)\mathbf{I} \tag{2}$$

and

$$\dot{\varepsilon}_p = \dot{\varepsilon}_0\left(\frac{\sigma_e}{g}\right)^{1/m} \tag{3}$$

Here, α denotes plastic compressibility parameter, $\dot{\varepsilon}_0$ is a reference strain rate, *m* stands for the rate hardening exponent and the hardness function $g\left(\varepsilon_p\right)$ is given by

$$g\left(\varepsilon_p\right)=\sigma_0\begin{cases}1+h_1\varepsilon_{p,} & \varepsilon_p \prec \varepsilon_1 \\ 1+h_1\varepsilon_1+h_2\left(\varepsilon_p-\varepsilon_1\right), & \varepsilon_1 \prec \varepsilon_p \prec \varepsilon_2 \\ 1+h_1\varepsilon_1+h_2\left(\varepsilon_2-\varepsilon_1\right)+h_3\left(\varepsilon_p-\varepsilon_2\right), & \varepsilon_p \succ \varepsilon_2\end{cases} \tag{4}$$

where, σ_0 indicates a reference stress. The effective stress, σ_e is defined by

$$\sigma_e^2=\frac{3}{2}\,\boldsymbol{\tau}:\mathbf{p}\,\frac{3}{2}\left[\boldsymbol{\tau}:\boldsymbol{\tau}\,-\alpha\left(tr\left(\tau\right)\right)^z\right] \tag{5}$$

The plastic dissipation per unit volume is

$$\boldsymbol{\tau}:\mathbf{d}^p=\sigma_e\dot{\varepsilon}_p \tag{6}$$

The effective stress, σ_e as defined in Eq. (5) has both hydrostatic as well as deviatoric components. To show this clearly, σ_e^2 in Eq. (5) can be rewritten as:

$$\sigma_e^2=\sigma_M^2+9\left(\frac{1-3\alpha}{2}\right)\sigma_h^2 \tag{7}$$

where

$$\sigma_M^2=\frac{3}{2}\tau':\tau', \qquad \sigma_h=\frac{1}{3}tr\left(\tau\right) \tag{8}$$

with

$$\tau'=\tau-\sigma_h\,\mathbf{I} \tag{9}$$

So, one can see that the plastic dissipation, Eq. (6) can also be written as:

$$\tau:\mathbf{d}^p=\frac{\dot{\varepsilon}_p}{\sigma_e}\left[\sigma_M^2+9\left(\frac{1-3\alpha}{2}\right)\sigma_h^2\right] \tag{10}$$

It is very clear from the above equation (10) that $\tau:\mathbf{d}^p$ is non-negative for all stress states when $\alpha\le 1/3$ and for $\alpha=1/3$, the constitutive equation becomes that of an isotropic hardening plastically incompressible Mises solid. The present study generates numerical results of two different materials *B* and *E* [13] for which the hardness functions, $g\left(\varepsilon_p\right)$ are plotted in Fig. 1. Material *B* is a bilinear hardening material and material *E* is a trilinear hardening-softening-hardening material. The parameters, $h_1=24$ and $\varepsilon_1=0.085$ are used for both the materials. The fixed parameters for the current analysis are $E/\sigma_0=100$, reference strain rate $\dot{\varepsilon}_0=1$ and rate hardening exponent *m*=0.02. For a quasi-static response, the values of parameters such as Young's modulus *E*, reference stress σ_0 etc do not separately affect the response, but the response depends on the values of appropriate ratios, [13].

We consider here an initially blunted crack. In the present work, the simulations are carried out for a semi circular region with radius R_0=2.0 in arbitrary units as shown in Fig. 2(a). There is a notch of initial radius,

b_0=0.001 in the same arbitrary units with its centre at the origin of the coordinate system, Fig. 2(b) so that R_0/b_0=2.0×10^3. Quadrilateral elements, each comprising of four "crossed" constant strain triangular elements have been employed for mesh generation. Such "crossed" elements, with a proper aspect ratio and orientation are widely used to reproduce localized deformation at finite strains, [17]. Isotropic linear elastic mode I crack tip field is prescribed on the outer boundary of the semi circular geometry in terms of displacements expressed in Eqs. (11) and (12).

$$\dot{u_1} = \frac{2(1+\nu)\dot{K}_1}{E}\sqrt{\frac{R}{2\pi}}\cos\left(\frac{\theta}{2}\right)\left[1-2\nu+\sin^2\left(\frac{\theta}{2}\right)\right] \tag{11}$$

and

$$\dot{u_2} = \frac{2(1+\nu)\dot{K}_1}{E}\sqrt{\frac{R}{2\pi}}\sin\left(\frac{\theta}{2}\right)\left[2-2\nu-\cos^2\left(\frac{\theta}{2}\right)\right] \tag{12}$$

where

$$R = \sqrt{\left(\left(y^1\right)^2+\left(y^2\right)^2\right)} \qquad \theta = \tan^{-1}\left(\frac{y^2}{y^1}\right) \tag{13}$$

and K_I, the stress intensity factor. The corresponding applied *J* value i. e. J_{app}, during small scale yielding, is given as:

$$J_{app} = K_I^2\left(1-\nu^2\right)/E \tag{14}$$

For the present simulation, $\left(K_I\right)_{\max}/K_{ref} = 1.34$ and $\left(K_I\right)_{\min}/K_{ref} = -0.67$ with $K_{ref} = \sigma_0\sqrt{1000b_0}$, so that the stress ratio (*R*) is - 0.5 and $\Delta K = 2.0$. For all load cycles a triangular shape waveform was used and there are total ten load cycles used in the simulation. A convected coordinate Lagrangian formulation of the field equations has been used in this present finite deformation finite element analysis. Similar formulation has widely been in use earlier, like in [10-11, 13, 15]. A constant value of $\dot{K}_I/\sigma_0\dot{\varepsilon}_0\sqrt{b} = 31.62$ is prescribed and this normalized loading rate corresponds to $\dot{K}_I = 1MPa\sqrt{ms}^{-1}$. For the calculation of the deformation history, a linear incremental update with time step size of 0.0002 is used. A rate tangent method is used for the constitutive update, [18]. Mesh density used in the present calculations is shown in Fig. 2. This study focuses the crack growth simulation only due to the effect of crack tip blunting, [17].

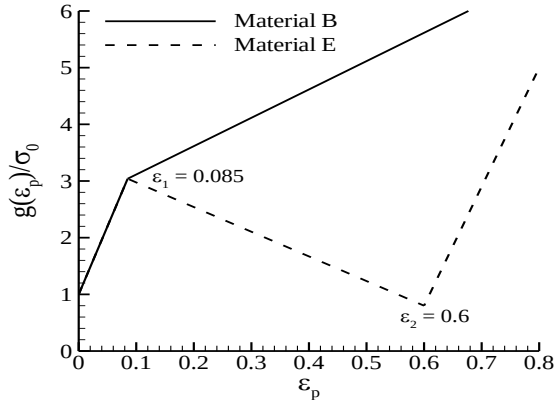

Fig.1
The hardness function $g\left(\varepsilon_p\right)$ as a function of plastic strain ε_p for material *B* (h_2= h_3= 5.0) and material *E* (h_2=-3.90, h_3=15.0, ε_2 = 0.6) [13].

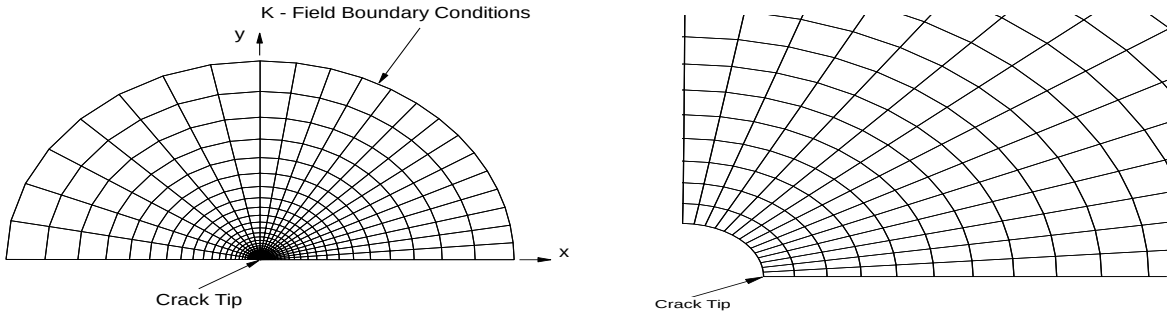

Fig.2
Typical mesh used in the finite element simulation of small scale yielding with K-field boundary conditions; a) Full mesh and b) Near tip mesh.

3 NUMERICAL RESULTS AND DISCUSSION

3.1 Mesh convergence

In computational fracture mechanics, for the global response convergence pertaining to mesh size, the two areas of interest are the crack tip region and the load application region. With the present visco-plasticity material model mentioned in section 2, mesh convergence study on the semi circular geometry under fatigue loading was carried out without any special crack tip element. In order to test the adequacy of the finite element mesh used, calculations were performed with mesh densities consisting of 22 × 54, 22 × 64, and 22 × 74 quadrilateral elements. Contours of plastic strain were compared in the near tip region for plastically incompressible material *B* (without overload) at the end of 10^{th} cycle, Fig. 3. It reveals that the plastic strain results from 22 × 64 and 22 × 74 are in very good agreement as compared to 22 × 54. Solutions were also obtained for other meshes and it was observed that except in the initial levels, the solutions were quite stable showing negligible differences at higher mesh densities. Comparing the solution accuracy and computation time, the final mesh density has been fixed at 22 × 64 rectangular elements with 1493 nodes. Near to the crack tip, sufficiently fine mesh is generated. The radial length of a finite element just next to the crack tip is roughly $b_0 / 40$.

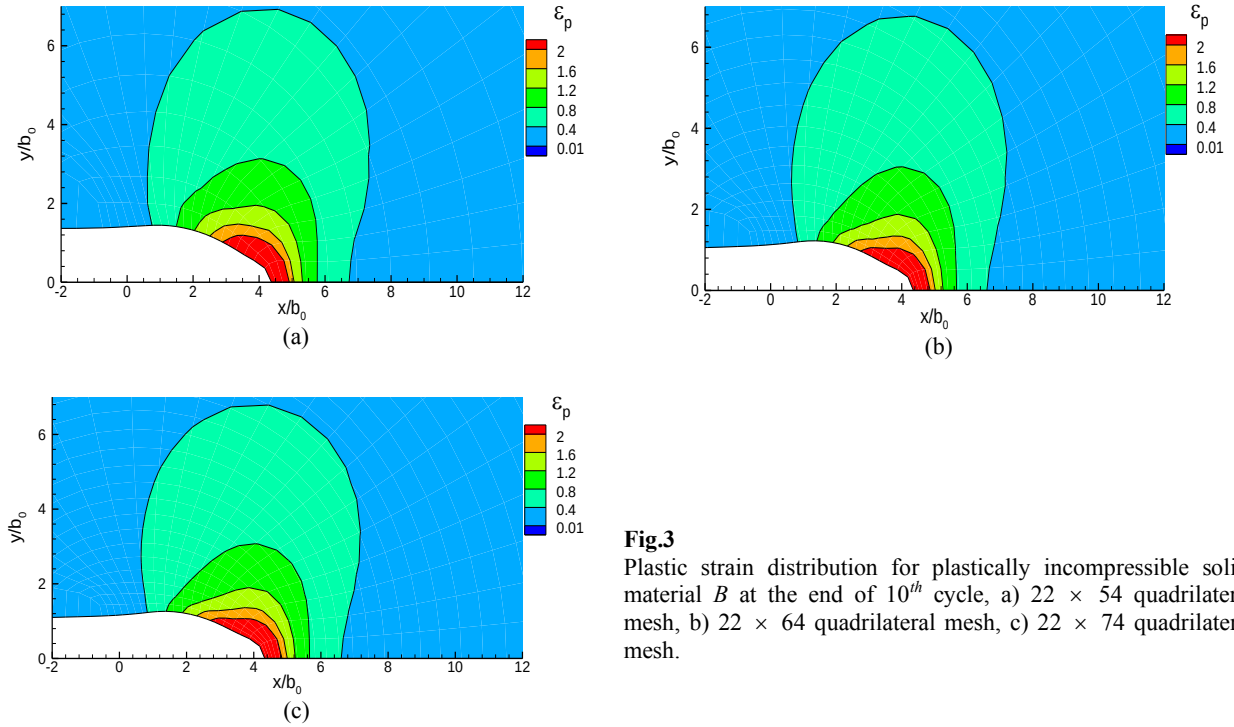

Fig.3
Plastic strain distribution for plastically incompressible solid, material *B* at the end of 10^{th} cycle, a) 22 × 54 quadrilateral mesh, b) 22 × 64 quadrilateral mesh, c) 22 × 74 quadrilateral mesh.

3.2 Comparison with earlier results

The accuracy of the present numerical results can be corroborated by noting the similarity of the near tip stress distributions for a propagating crack of Liu and Drugan [19] under monotonic loading. Liu and Drugan [19] used linear elastic - perfectly plastic material model with Young's modulus as 200 *GPa*, Poisson's ratio as 0.5 and yield stress as 1.173 *GPa*. Using identical conditions, the finite element simulation has been run with the present code and subsequently the normal and shear stresses are plotted in Fig. 4. The maximum σ_{xx} and σ_{yy} values (approximately 1.6 and 2.6, respectively) are almost matching with those of Liu and Drugan [19]. The distribution pattern of all the stress quantities is also almost similar. The minute discrepancy may be owing to dissimilar finite elements used for meshing. Liu and Drugan [19] have used conventional quadrilateral elements in their analysis whereas in the present study quadrilateral elements with crossed triangles have been employed. The results obtained in Fig. 4 encourage us to continue additional investigations.

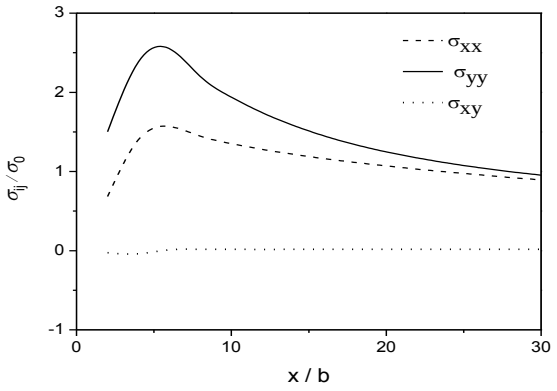

Fig.4
Stress distribution for a growing crack (with $\Delta a = 0.0086\left(K_I/\sigma_0\right)^2$ in an elastic-perfectly plastic material; the material properties are taken from Liu and Drugan [19].

3.3 Plastic crack tip advancement

In literature it has been claimed in recent times that negative stress ratio influences the fatigue crack growth significantly. In order to check this proposition for plastically compressible materials, the normalized crack extension versus normalized time of materials B and E for constant amplitude loading as well as that for variable amplitude loading (with overload at the fifth cycle; $K_{overload} = 2.0\,\mathrm{K_{max}}$ have been plotted in Figs. 5 – 6, respectively. Here, time (t) has been normalized by $t_0\left(=\varepsilon_0/\dot{\varepsilon}_0\right)$, where $\varepsilon_0\left(=\sigma_0/E\right)$ indicates the yield strain. Initially, attention is focused for constant amplitude loading, Fig. 5(a) and Fig. 6(a). When the material is plastically incompressible, it is evident that the maximum crack growth takes place during the first cycle in both the cases and then it rises with lower rate. The growth in the first loading cycle is more in material E as compared to that of material B; in material B in the subsequent cycles also growth amount is significant but this is not so in material E. This present crack growth nature is in sharp contrast to the cases when stress ratio is positive and zero, [17]. It is observed that in material B (plastically compressible) at the end of loading phase of each cycle the difference in the amount of crack growth is a small amount though the same difference is more at the end of unloading phase of each cycle. This difference, during the unloading phase, increases with increase in plastic compressibility. Such behavior was not observed for positive and zero stress ratio, [17]. In material E on the other hand plastic compressibility leads to significant amount of crack growth reduction though there is a tendency of continuous increase of the crack growth. The overall crack extension is highest in plastically incompressible material E. This increase of fatigue crack growth at negative stress ratio may be resulting from the reverse plastic yielding near the crack tip during compressive loading. In case of positive and zero stress ratio, this reverse plastic yielding is absent and therefore, fatigue crack growth is less influenced. At negative stress ratio, near the crack tip, the crack is not entirely closed as will be observed from the following CTOD figures, thus, there are stress concentration and reverse plastic yielding caused by the applied compressive load near the crack tip. This is also revealed in the works of Bai et. al. [4]. It is also to be noted interestingly here that in material E (plastically compressible) when the value of $\alpha = 0.25$, initially for a few cycles at the end of unloading phase, the crack tip moves in the negative x direction with respect to the original crack tip location. It is further to be mentioned here that the present simulations have also been run with constant amplitude load for the negative stress ratio of -1.0 and the nature of the results obtained in material E is

qualitatively same and only difference is that the reduction in the growth rate is more with increase in the number of cycles for $\alpha = 0.25$. For material B as there was touching of the crack faces, we did not extend the simulation.

The crack growth is very much sensible to an overload and this also halts the crack advancement, Fig. 5(b) and Fig. 6(b). It is very much clear that up to the 4^{th} cycle there is rising nature in the crack growth curve; during the overload the crack growth shoots up but after the overload cycle the crack growth is reduced and almost constant. In material B (Fig. 5(b)), the rate of rise is very sharp and it is nearly same for all the crack growth curves though the amount of rise varies because of the plastic compressibility. It is also evident that with increase in the plastic compressibility, there is increase in the fall of the crack growth curve during the unloading phase of the overload cycle and during the pre-overload cycles differences are not so much as observed in Fig. 5(b). In material E, with increase in plastic compressibility one can observe that even during the overload cycle the crack growth increases only a little as compared to the other cases and this is very interesting observation. In the present study, during post-overload cycles, crack growth is decreased and it is almost constant throughout; there is a bit delayed retardation. Reason for the retarded crack growth after the overload cycle may be the plastic deformation of the crack tip, crack tip blunting, bigger plastic zone size during the application of overload etc. It has been observed in some of our earlier publications [15,17] that plastic compressibility leads to bigger plastic zone in front of a crack tip as compared to the situation when the material is plastically incompressible. Also it has been observed in those reported works [15,17] that softening tends to intensify and localize the plastic deformation near the crack tip. Therefore, it can be concluded here that the combination of plastic compressibility and material softening helps to reduce the crack growth significantly. This may be a very significant conclusion towards the development of any new material.

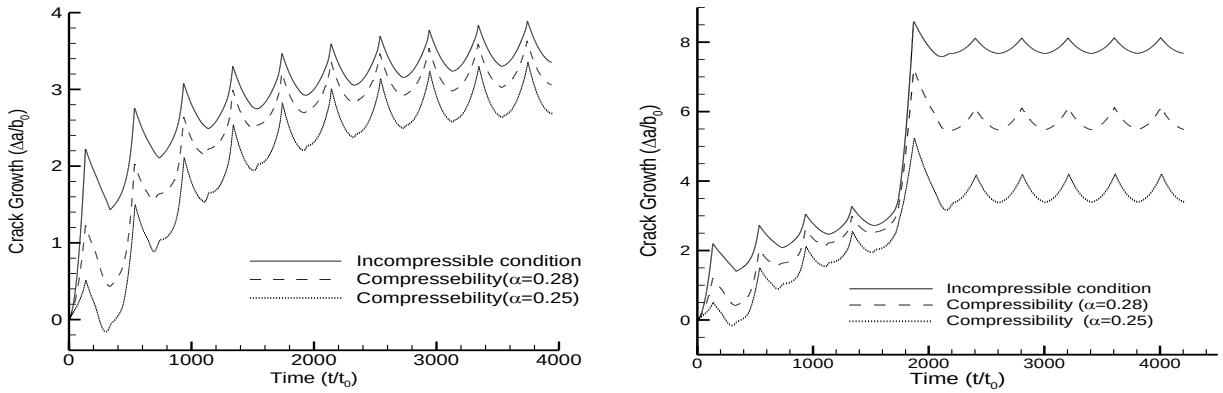

(a) (b)

Fig.5

Normalized crack extension ($\Delta a/b$) versus normalized time (t/t_0) of material B for stress ratio (R) = - 0.5 (a) without overload; (b) with overload.

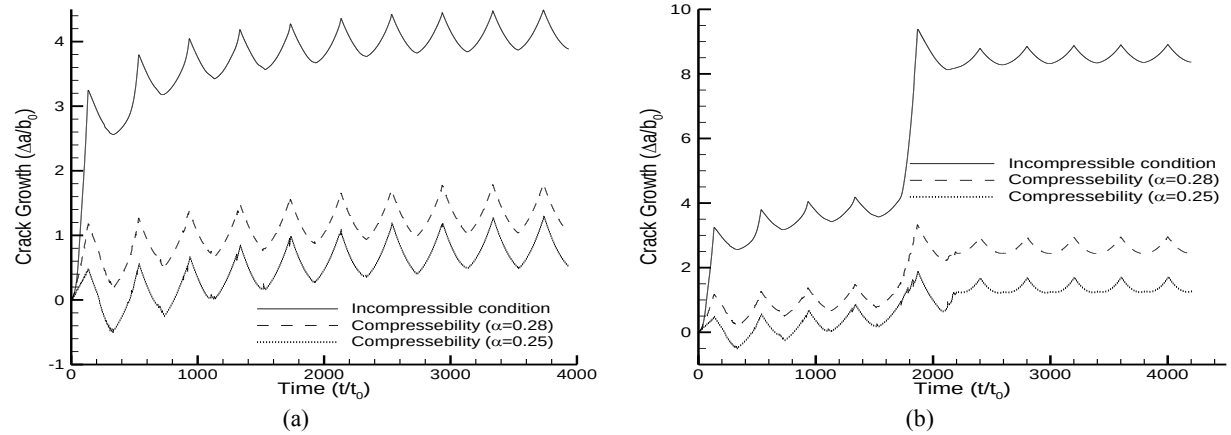

(a) (b)

Fig.6

Normalized crack extension ($\Delta a/b$) versus normalized time (t/t_0) of material E for stress ratio (R) = - 0.5 (a) without overload; (b) with overload.

3.4 Crack tip opening displacement

Other than the crack tip growth another important parameter for the crack tip deformation is the CTOD. Fig. 7 illustrate the CTOD variation against applied loading at negative stress ratios of R = - 0.5 for materials B and E and when the value of compressibility parameter is 0.28. Initially, with increase in the number of cycles crack opening is increasing slowly in material B whereas in material E, the CTOD is decreasing very fast before the convergence of cyclic CTOD trajectories to steady state and self similar loops is attained. For positive and zero stress ratio it has been observed that the convergence of the CTOD trajectories to steady state and self similar loops is very fast for material B and slightly delayed in material E, [17]. For material E whose hardness function is hardening-softening-hardening in nature there are more or less abrupt jumps observed in the CTOD values during the loading phase and this may be because of the evolution of region of localized deformation that develops in the front of crack tip. The abrupt jumps in the CTOD values depend on stress ratio; for negative stress ratio, the jump is more in comparison to the positive and zero stress ratios, [17]. It is also clear that crack closure is not there in any of the load cycles even for the negative stress ratio.

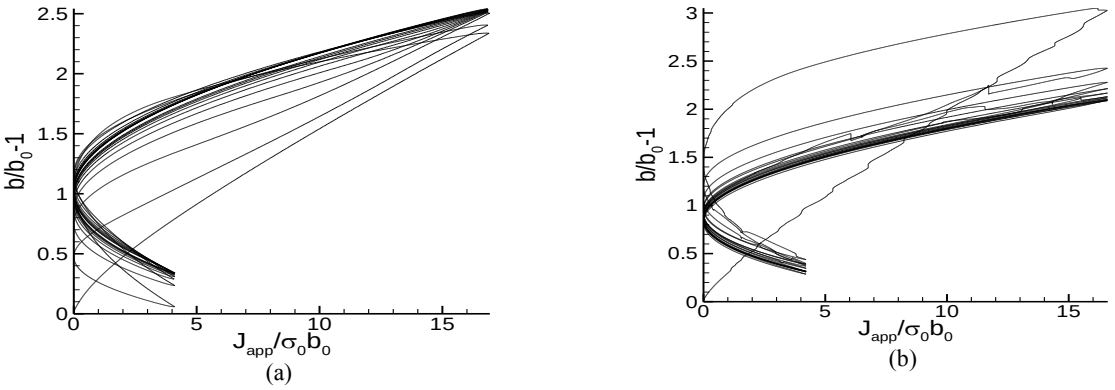

Fig.7
Crack-tip opening displacement $\delta_t (= b/b_0 - 1)$ versus applied J-integral, J_{app} with $K_{\max} = 1.34$ and $K_{\min} = -0.67$ for plastically compressible solid, $\alpha = 0.28$ (up to 10^{th} cycle); (a) material B (b) material E.

3.5 Distribution of normal stress (σ_{yy}) along the symmetry plane

Figs. 8 – 9 illustrate the distribution of crack opening stress σ_{yy} ahead of the tip along the symmetry plane at low and high peak loads during pre (4^{th}) and post (6^{th}) overload cycles for the materials B and E. From all these figures, one can observe that near-tip σ_{yy} stresses vary along the symmetry plane and also the stress fields are influenced by plastic compressibility and strain softening. Very far from the tip, the stress distribution becomes nearly invariable. Absolute tensile and compressive stress values are maximum for each figure when the material is plastically incompressible. During the pre overload cycle (i. e. 4^{th} cycle) the near tip stress distributions are approximately self-similar in nature at least when the material is plastically incompressible. With increase in plastically compressibility sharpness in the peak value of σ_{yy} is decreasing for both $K \to K_{\max}$ and $K \to K_{\min}$. The absolute tensile and compressive extremes of stress for the plastically incompressible solids are attained at corresponding high and low peak loads, and these are, respectively, $\left(\sigma_{yy}\right)_{\max} = 6$ and $\left(\sigma_{yy}\right)_{\min} = -6$, Fig. 8(a). These extreme values are reduced with increase in plastic compressibility. The reason behind this may be the increase of plastic zone size in presence of plastic compressibility. The results of the plastically incompressible solids are matching in a qualitative way with the results of Toribio and Kharin, [14]. Next, in material E where there is material softening followed by hardening, the self similarity of the near tip stress distributions is destroyed at least for the plastically compressible solid corresponding to $K \to K_{\max}$ and $K \to K_{\min}$. Moreover, for material E and when it is plastically compressible, Fig. 8(b), oscillations are observed in the stress distributions and the cause of this possibly may be the intense plastic straining emanating from the crack tip, [15]. Material softening tends to build up and confine the plastic deformation near the tip only. Also in material E, maximum normal stress is located a little away from the tip. The stress distribution for the post overload cycle is not self-similar even for the hardening material B. Here the absolute compressive extreme of stress is more as compared to the absolute tensile extreme of stress for both the

materials. Significant oscillations are observed in the stress distributions of plastically compressible material *E*. It is also observed from Fig. 9(b) that for plastically compressible material the residual compressive stress in the post overload cycle is significantly more as compared to that of the pre overload cycle which may be one of the reasons behind the crack growth reduction.

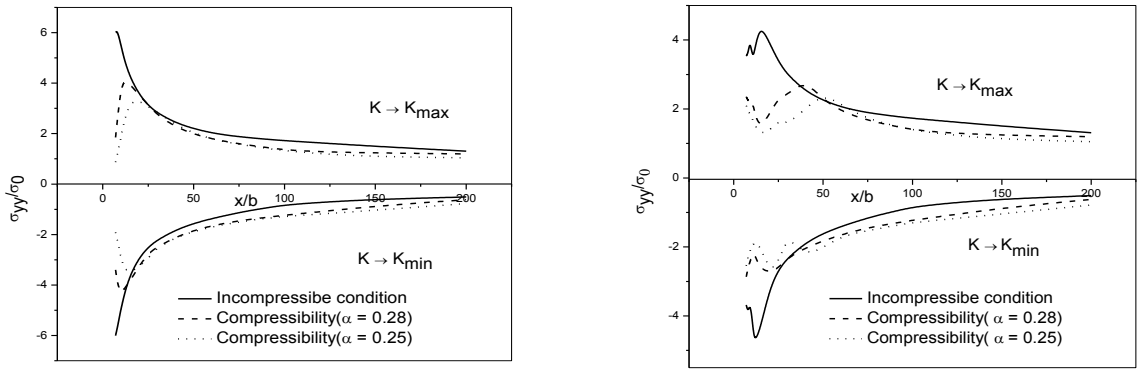

(a) (b)

Fig.8
Distribution of the near-tip normal stress σ_{yy} along the symmetry plane for at high and low peak loads during 4^{th} cycle; stress ratio -0.5; (a) material *B* (b) material *E*.

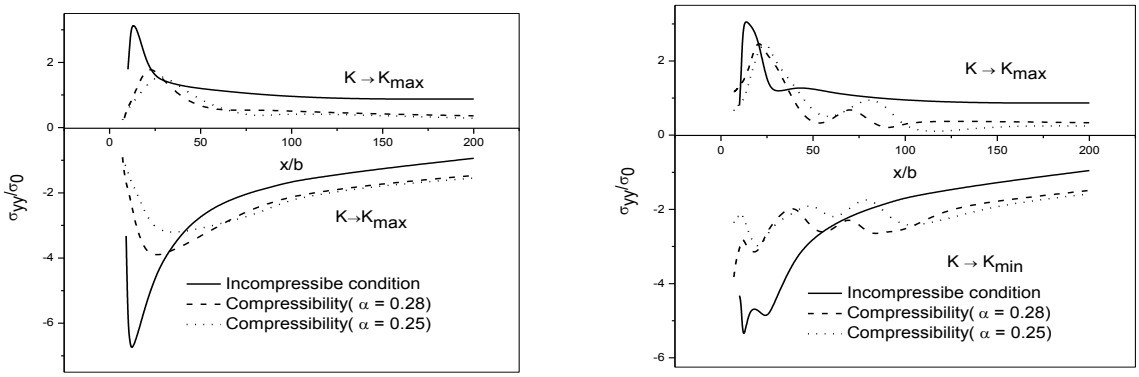

(a) (b)

Fig.9
Distribution of the near-tip normal stress σ_{yy} along the symmetry plane for at high and low peak loads during 6^{th} cycle; stress ratio -0.5; (a) material *B* (b) material *E*.

4 CONCLUSIONS

In this study, an investigation is conducted on the role of negative stress ratio, plastic compressibility and material softening on fatigue crack growth by using a finite strain elastic viscoplastic constitutive model and finite element method. The following conclusions can be drawn from the current study:

- In a sharp contrast to the crack growth under positive and zero stress ratios, crack grows continuously for both the materials under negative stress ratio with respect to time though the growth is more for the hardening material. When there is increased plastic compressibility, it is revealed that during the unloading phase of the initial few cycles crack tip moves in the negative *x* direction with respect to the initial crack tip location for the hardening-softening-hardening solid. Overload does not alter the crack growth much during the loading time for the hardening-softening-hardening solid. The combination of plastic compressibility and material softening leads to substantial amount of crack growth reduction.
- Though CTOD is increased in presence of plastic compressibility under monotonic loading but during fatigue loading with negative stress ratio CTOD is significantly reduced when plastic compressibility is

combined with strain softening.

- As the plastic zone size is increased due to of plastic compressibility; intense strain region originates from the crack surface close to the symmetry line due to material softening and there is reverse plastic yielding caused by the applied compressive load, the normal stress (σ_{yy}) becomes very sensitive to plastic compressibility, material softening and negative stress ratio.
- For development of foam/VACNTs/polymer kind of material where there is plastic compressibility and material softening just after yield and then progressive rehardening, the present analysis will give a good guideline.

REFERENCES

[1] Carlson R.L., Kardomateas G.A., 1994, Effects of compressive load excursions on fatigue crack growth, *International Journal of Fatigue* **16**: 141-146.

[2] Silva F.S., 2005, The importance of compressive stress ratio on fatigue crack propagation, *International Journal of Fatigue* **27**: 1441-1452.

[3] Zang J., He X.D., Sha Y., Du S.Y., 2010, The compressive stress effect on fatigue crack growth under tension-compression loading, *International Journal of Fracture* **32**: 361-367.

[4] Bai S., Sha Y., Zhang J., 2018, The effect of compression loading on fatigue crack propagation after a single tensile overload at negative stress ratios, *International Journal of Fatigue* **110**: 162-171.

[5] Benz C., 2018, Fatigue crack growth at negative stress ratios: on the uncertainty of using ΔK and R to define the cyclic crack tip load, *Engineering Fracture Mechanics* **189**: 194-203.

[6] Hassanifard S., Bonab M.A., Mohtadi M., Jabbari G.h., 2013, Investigation of fatigue crack propagation in spot-welded joints based on fracture mechanics approach, *Journal of Materials Engineering and Performance* **22**: 245-250.

[7] Bonab M.A., Mohtadi M., Eskandari M., Ghaednia H., Das S., 2016, Effect of microstructural parameters on fatigue crack propagation in an API x65 pipeline steel, *Journal of Materials Engineering and Performance* **25**: 4933-4940.

[8] Rudnicki J. W., Rice J. R., 1975, Conditions for the localization of deformation in pressure-sensitive dilatant material, *Journal of the Mechanics and Physics of Solids* **23**: 371-394.

[9] Spitzig W. A., Richmond O., 1979, Effect of hydrostatic pressure on the deformation behavior of polyethylene and polycarbonate in tension and compression, *Polymer Engineering and Science* **19**(16): 1129-1139.

[10] McMeeking R.M., 1977, Finite deformation analysis of crack tip opening in elastic-plastic materials and implications for fracture, *Journal of the Mechanics and Physics of Solids* **25**: 357-381.

[11] Hutchens S.B., Needleman A., Greer J.R., 2011, Analysis of uniaxial compression of vertically aligned carbon nanotubes, *Journal of Mechanics and Physics of Solids* **59**: 2227-2237.

[12] Needleman A., Hutchens S.B., Mohan N., Greer J.R., 2012, Deformation of plastically compressible hardening–softening–hardening solids, *Acta Mechanica Sinica* **28**: 1115-1124.

[13] Mohan N., Cheng J., Greer J.R., Needleman A., 2013, Uniaxial tension of a class of compressible solids with plastic non-normality, *Journal of Applied Mechanics* **80**: 040912-1-8.

[14] Toribio J., Kharin V., 2009, Finite deformation analysis of crack tip fields under cyclic loading, *International Journal of Solids and Structures* **46**(9): 1937-1952.

[15] Khan D., Singh S., Needleman A., 2017, Finite deformation analysis of crack tip fields in plastically compressible hardening-softening-hardening solids, *Acta Mechanica Sinica* **33**(1): 148-158.

[16] Lai J., Van der Giessen E., 1997, A numerical study of crack-tip plasticity in glassy polymers, *Mechanics of Materials* **25**: 183-197.

[17] Singh S., Khan D., 2018, On fatigue crack growth in plastically compressible hardening and hardening-softening-hardening solids using crack tip blunting, *International Journal of Fracture* **213**: 139-155.

[18] Peirce D., Shih C.F., Needleman A., 1984, A tangent modulus method for rate dependent solids, *Computers & Structures* **18**(5): 875-887.

[19] Liu N., Drugan W.J., 1993, Finite deformation finite element analyses of tensile growing crack fields in elastic-plastic material, *International Journal of Fracture* **61**: 189-210.